Dynamic Response of Saturated Dense Sand in Laminated Centrifuge Container

Ahmed Elgamal, M.ASCE[1]; Zhaohui Yang, A.M.ASCE[2]; Tao Lai[3]; Bruce L. Kutter, M.ASCE[4]; and Daniel W. Wilson, A.M.ASCE

Abstract: A highly instrumented centrifuge experiment was conducted at the Univ. of California at Davis, to investigate the seismic response of a saturated dense sand stratum. Nevada sand at about 100% relative density was employed in a laminated (flexible shear beam) container to simulate one-dimensional site response. Among the total of 27 imparted earthquake-like shaking events, peak accelerations near ground surface ranged from 0.03 to 1.7*g* (in prototype scale), covering linear to highly nonlinear scenarios. This comprehensive set of recorded downhole accelerations is utilized herein to identify variation of shear modulus and damping ratio with shear strain amplitude. The estimated modulus reduction and damping ratio display a confinement dependence. At shear strains below about 0.2%, modulus variation is found in reasonable agreement with the formulae of Hardin–Drnevich and the modulus reduction bounds of Seed–Idriss, while damping is generally higher. At shear strains larger than 0.2%, the shear-induced dilation tendency maintained secant shear modulus at about 20% of its initial value, with a 20% damping ratio approximately. In earlier laboratory experimental studies on loose to medium-dense sands, Vucetic and Matasovic also reported similar trends. Based on the findings, a two-phase (solid and fluid) fully coupled nonlinear finite element program is calibrated and used to conduct numerical simulations of representative weak to strong shaking events. The computational results are in good agreement with the recorded counterparts, and satisfactorily reproduce the important dilation effects.

DOI: 10.1061/(ASCE)1090-0241(2005)131:5(598)

CE Database subject headings: Sand; Saturated soils; Centrifuge model; Damping ratio; Dilatancy; Soil dynamics; Amplification.

Introduction

In January 1998, the Southern California Earthquake Center organized a workshop on nonlinear seismic site response (Field et al. 1998). Discussions among seismologists and geotechnical engineers during this workshop revealed different opinions as to the extent of nonlinear response, particularly for stiff soil sites. Adequacy of equivalent linear procedures and the need for fully nonlinear analyses were among the outstanding questions.

Motivated by the workshop discussions, a collaborative effort to investigate the dynamic response of stiff soil sites was initiated between the Univ. of California at Davis (UCD) and the Univ. of California at San Diego (UCSD). Such stiff site studies are of significance for many urban areas worldwide and particularly for southern California. The UCD team conducted highly instrumented physical model tests (on a large centrifuge), to determine the behavior of stiff soil sites (dense sand) under low to high levels of seismic excitation (Stevens 2001; Stevens et al. 2001a,b). At UCSD, attention was directed towards analysis and numerical simulation of the UCD centrifuge testing results (Elgamal and Lai 2001, Lai et al. 2001, 2002).

In this paper, data from one of the UCD centrifuge experiments (DKS04, Stevens et al. 2001a) was employed to study the dynamic response of a saturated dense sand stratum. A laminated container was used in the experiment to reduce the two-dimensional (2D) lateral boundary effects, and more closely simulate 1D site response. The recorded downhole acceleration time histories at different depths along the model centerline (where 1D response is dominant) were first employed to back-calculate shear stress and shear strain response. This stress-strain data was then utilized to identify the stiffness, damping, and dilatancy characteristics of the saturated stiff soil deposit. Finally, numerical simulations were performed for representative weak to strong shaking events, using a solid–fluid fully coupled finite element (FE) program (England et al. 2002, 2003, Yang and Elgamal 2002). In the following section, we start with a brief description of the experimental setup and recorded data.

Centrifuge Experiment

Centrifuge Model Configuration

The experiment (DKS04) was conducted in a flexible shear beam (FSB) container mounted on the 9 m radius geotechnical centri-

[1]Professor, Dept. of Structural Engineering, Univ. of California at San Diego, La Jolla, CA 92093.

[2]Assistant Project Scientist, Dept. of Structural Engineering, Univ. of California at San Diego, La Jolla, CA 92093.

[3]Applied Insurance Research Worldwide Corporation, 131 Dartmouth St., Boston, MA 02116.

[4]Professor, Dept. of Civil and Environmental Engineering, Univ. of California at Davis, Davis, CA 95616.

[5]Research Engineer, Dept. of Civil and Environmental Engineering, Univ. of California at Davis, Davis, CA 95616.

Note. Discussion open until October 1, 2005. Separate discussions must be submitted for individual papers. To extend the closing date by one month, a written request must be filed with the ASCE Managing Editor. The manuscript for this paper was submitted for review and possible publication on July 7, 2003; approved on August 20, 2004. This paper is part of the ***Journal of Geotechnical and Geoenvironmental Engineering***, Vol. 131, No. 5, May 1, 2005. ©ASCE, ISSN 1090-0241/2005/5-598–609/$25.00.

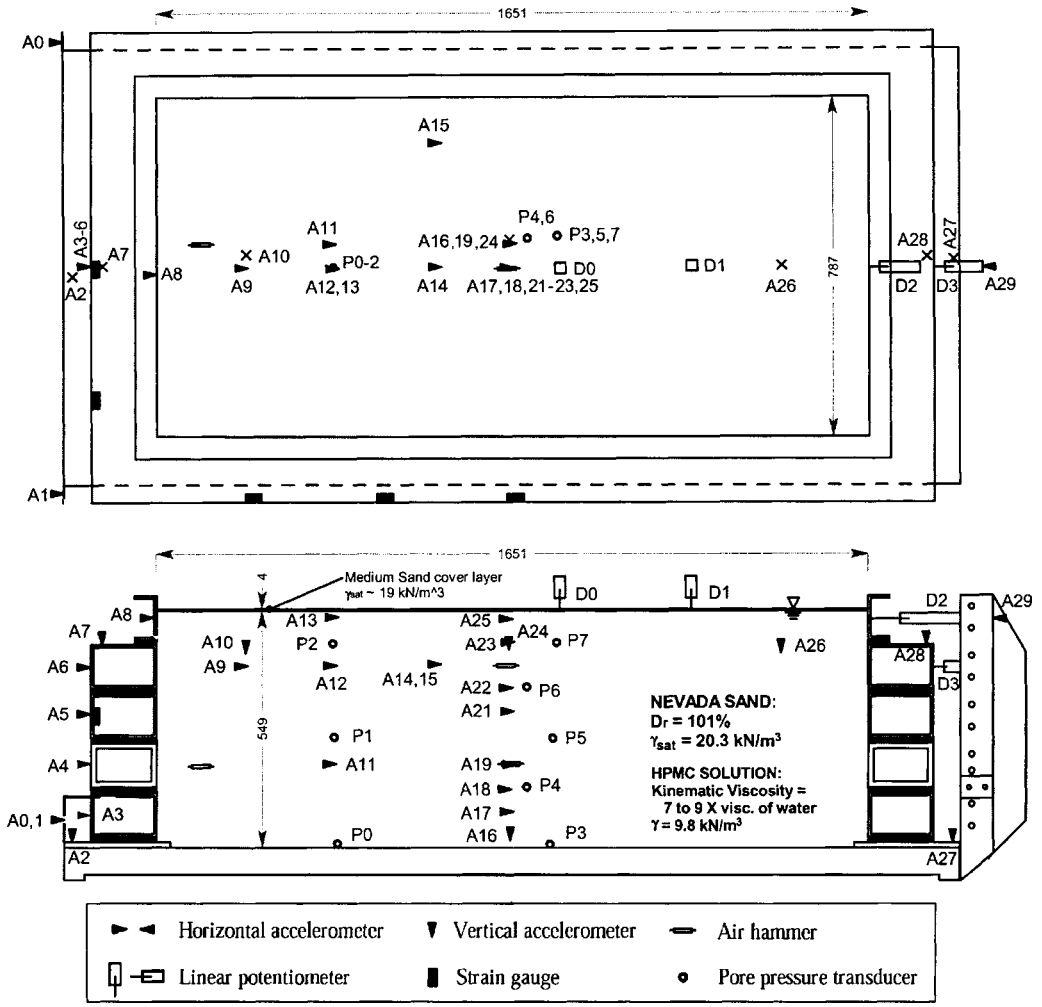

Fig. 1. DKS04 centrifuge test series model configuration in flexible shear beam container (container dimensions are in millimeters, after Stevens et al. 2001a)

fuge at UCD (Kutter et al. 1991). This FSB container consists of a rigid base plate and five rigid rings, with overall dimensions of $1.651 \times 0.787 \times 0.553$ m in length, width, and height, respectively (Fig. 1). The container rings are sandwiched with soft rubber interfaces providing lateral flexibility. Dynamic excitation was imparted primarily along the longitudinal direction. This testing configuration mimics the 1D vertical shear wave propagation condition (shear beam response). As shown in Fig. 1, the model was instrumented with extensive horizontal and vertical arrays of accelerometers, piezometers, and potentiometers.

Nevada sand at about 100% relative density (D_r) was used to represent a stiff soil formation (sand properties are documented and discussed in Arulmoli et al. 1992 and Stevens 2001). This very dense stratum was prepared by air-pluviating sand to a D_r of approximately 90% in about 60 mm lifts (model units). Each lift was leveled and compacted using a surface vibrator to reach the final D_r (see Stevens et al. 2001a for more details). Unit weight of the saturated sand and the pore fluid were 20.3 and 9.8 kN/m^3, respectively. A pore-fluid with viscosity equal to about eight times that of water was employed, resulting in a prototype permeability coefficient within the range of medium to fine sands (Lambe and Whitman 1969).

Using buried air hammers (Fig. 1), over 75 low-amplitude shear wave pulses were generated, and the corresponding shear wave velocity was determined by a cross-correlation analysis of pulse travel time (Stevens 2001, Stevens et al. 2001b). For the purpose of this study, the representative shear velocity profile was defined to be $V_s(z) = 124\, z^b$ (m/s), in which z is the depth coordinate in meters, and $b = 0.25$ dictates a smooth variation of V_s with depth. The low-strain shear modulus G_{max} profile follows from the relationship $G_{max} = \rho V_s^2$ where ρ is saturated mass density.

Shaking Events and Data Sets

The model in Fig. 1 was subjected to 27 earthquake-like shaking events. These events were imparted at centrifugal acceleration levels of 9.2, 18.1, 25.3, and 37.3g, representing a prototype stratum of 5.1, 10.0, 14.0, and 20.6 m depth respectively (scaling factors relating model to prototype are shown in Table 1, after Kutter 1992). The input excitations were scaled versions of the Santa Cruz ground motion (90°) recorded during the 1989 Loma Prieta earthquake, and a scaled version of the Port Island ground motion (83 m depth, NS component) recorded during the 1995 Kobe earthquake. Sequence of the imparted shaking events (Table 2) was documented in Stevens (2001) and Stevens et al. (2001a). It was found that this shaking sequence caused further densifica-

Table 1. Scaling Factors of Model Dimension to Prototype Dimension at the Centrifugal Acceleration (g) Level of n (after Kutter 1992)

Quantity	Model dimension	Prototype dimension
Mass density	1	1
Displacement, distance	1	n
Dynamic time	1	n
Frequency	1	$1/n$
Acceleration	1	$1/n$
Velocity	1	1
Force	1	n^2
Mass	1	n^3
Stress	1	1
Strain	1	1
Permeability	1	n

tion of the sand stratum, resulting in about 10% increase of initial low-strain shear modulus (accounted for by the shear wave velocity profile adopted above).

Table 2 lists peak acceleration at *A*25 (near the surface, Fig. 1) and *A*17 (near the base) for all 27 shaking events. Near the model surface, recorded peak acceleration in the longitudinal direction ranged from 0.03 to 1.73g (in prototype scale). As will be shown, this wide range of peak acceleration resulted in soil response covering linear to highly nonlinear scenarios.

Identification of Dynamic Soil Properties

Observed Response Characteristics

Representative acceleration and pore-water pressure time histories of a strong shaking event (Event 41) are depicted in Fig. 2. Similar to all other events, the relatively fast dynamic excitation occurs under practically undrained conditions. In Fig. 2, peak excess pore pressure ratio r_u ($=u_e/\sigma'_v$ where u_e is excess pore pressure and σ'_v is initial effective vertical stress) remained relatively low at most monitored locations, ranging from 0.2 at depth to about 0.4 near ground surface. This pore pressure increase corresponds to only 10–20% reduction in low-strain shear modulus G_{max} (Stevens et al. 2001b).

Close inspection of Fig. 2 indicates that most high acceleration peaks coincide with an instantaneous reduction in pore pressure. This phenomenon is a direct consequence of the shear-induced

Table 2. *UCD DKS04* Shaking Events and Peak Acceleration (Units in Prototype Scale;Stevens 2001)

Number[a]	Event ID	Peak acceleration (g) A25	Peak acceleration (g) A17	Centrifuge g level (model depth)	Depth of central vertical array accelerometers (m)
1	DKS04_01	0.101	0.022		
2	DKS04_02	0.168	0.046		
3	DKS04_03	0.481	0.170		
4	DKS04_04	0.154	0.086	9.19g (5.08 m)	0.22, 0.71, 1.69, 2.20, 3.32, 3.85, 4.32[b]
5	DKS04_05	0.076	0.024		
10	DKS04_34	0.828	0.493		
11	DKS04_35	0.443	0.276		
12	DKS04_40	0.897	0.641		
13	DKS04_41	0.859	0.526		
14	DKS04_44	0.211	0.125		
15	DKS04_48	0.519	0.361		
16	DKS04_49	0.385	0.260		
17	DKS04_50	0.155	0.108	18.13g (10.03 m)	0.43, 1.40, 3.34, 4.33, 6.55, 7.60, 8.53[b]
18	DKS04_51	0.905	0.634		
19	DKS04_52	0.412	0.327		
26	DKS04_69	—[c]	1.261		
27	DKS04_70	—[c]	1.144		
6	DKS04_13	0.080	0.020		
7	DKS04_14	0.045	0.012		
8	DKS04_15	0.043	0.020	25.28g (13.98 m)	0.59, 1.95, 4.65, 6.04, 9.14, 10.59, 11.89[b]
9	DKS04_16	0.031	0.014		
20	DKS04_55	0.579	0.412		
21	DKS04_56	0.369	0.244		
22	DKS04_59	0.792	0.537		
23	DKS04_62	0.330	0.194	37.33g (20.64 m)	0.88, 2.87, 6.87, 8.92, 13.49, 15.64, 17.56[b]
24	DKS04_63	0.148	0.072		
25	DKS04_66	0.209	0.087		

[a]Sequence of imparted shaking events.

[b]Depth of accelerometers *A*25, *A*23, *A*22, *A*21, *A*19, *A*18, and *A*17 respectively.

[c]Out of range.

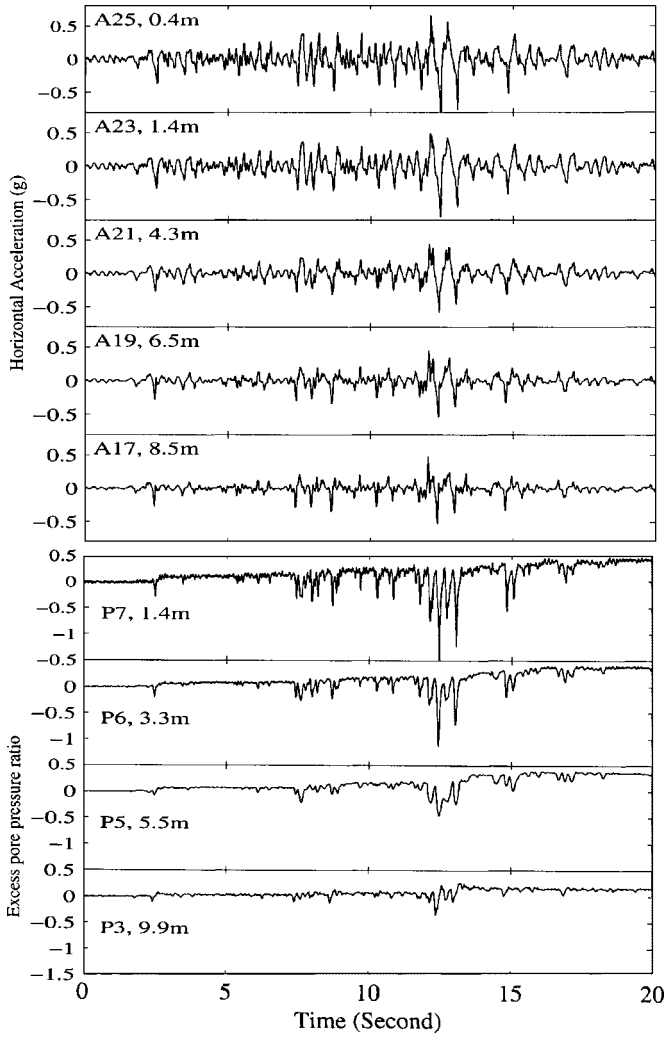

Fig. 2. Event 41 acceleration and pore pressure time histories

dilation tendency (Lambe and Whitman 1969). The significant influence of dilation on undrained shear stress-strain response and associated dynamic soil properties will be thoroughly addressed below.

Shear Stress–Strain Histories

Attention was focused on events where 1D shear behavior was dominant (Lai et al. 2001, 2002). The calculation of shear stress and shear strain histories followed the procedure of Koga and Matsuo (1990), Zeghal et al. (1995), and Elgamal et al. (1996). Assuming a 1D vertically propagating shear wave, shear stress and shear strain response at a particular depth can be estimated using the recorded lateral downhole accelerations (Koga and Matsuo 1990, Zeghal et al. 1995). This estimate is of second order accuracy, and is representative of average response midway between the accelerometer stations. In this 1D scenario, effect of the container mass on shear stress was accounted for by a 24% increase in the employed soil mass density (total mass of the container laminates is about 24% of the total saturated sand mass in the container, Stevens et al. 2001a).

The calculated shear stress–strain histories at the accelerometer locations along the centerline are shown in Fig. 3 for three shaking events (15, 49, and 41), representative of weak, moderate, and strong shaking conditions respectively. In all three cases, the initial low-strain shear stiffness is seen to gradually increase with depth, indicating confinement dependence (Zeghal et al. 1995). In the weak event (Event 15) with maximum shear strain in the range of about 0.01%, the shear stress–strain response remained essentially linear throughout, with minimal associated damping (measured as the area enclosed by the stress–strain loops). In the moderate event (Event 49) with maximum shear strain in the range of about 0.2%, soil nonlinearity becomes significant as the shear stiffness decreases with the increase in shear strain. This nonlinear response is associated with a considerable level of damping. In the strong event (Event 41) with maximum shear strain in the range of about 0.5%, modulus reduction with strain is also evident. However, at shear strain beyond about 0.3% (Fig. 4), the tangent shear stiffness tends to remain constant or even increase. Such regain in stiffness (and strength) at large shear strain levels is due to the associated dilative tendency, as typically observed in laboratory experiments of medium-to-dense sands (e.g., Ishihara 1985, Fig. 5).

Dilative Response Mechanism and Related Effects

At large shear strain excursions, dense granular soils tend to dilate (Lambe and Whitman 1969). In an effective-stress-path diagram (Figs. 5 and 6), the phase transformation angle (Ishihara et al. 1975, Ishihara 1985) delineates the boundary between contractive and dilative response. Under undrained conditions [Fig. 6(a)], dilation will cause (Vucetic 1986; Matasovic and Vucetic 1993): (1) increase in effective confinement or reduction in pore pressure (Fig. 2) and (2) a corresponding increase in shearing resistance (stiffness and strength). This increasing shear resistance may lead to the appearance of acceleration spikes during dynamic excitation (Fig. 2, Kutter and Wilson 1999; Kramer and Elgamal 2001; Elgamal et al. 2001).

During shear loading, the above dilation effects will not be pronounced if the soil is dry or if drained conditions prevail, with minor change in effective confinement [Fig. 6(b)]. In these cases, stiffness gradually decreases with the increase in shear strain amplitude (Hardin and Drnevich 1970, 1972).

Variation in Shear Modulus and Damping Ratio

The evaluated shear stress–strain histories (Fig. 3) were utilized to estimate dynamic soil properties in terms of the conventional equivalent (secant) shear modulus (G) and damping ratio (ξ) curves (Seed and Idriss 1970). The procedure for estimating these properties is shown schematically in Fig. 7 (Kramer 1996). Data from two medium events (49 and 52) and three of the strongest events (41, 69, and 70) were used in this analysis phase. These events provided representative data at different confinement levels, with shear strain ranging from 0.001 up to about 1.0%.

Shear Modulus

Fig. 8 displays the G/G_{max} data evaluated from selected shear stress–strain loops at two depths, one near the surface (1.4 m) and the other near the base (7.6 m). The employed G_{max} was defined based on the employed shear wave velocity profile mentioned earlier. Fortunately, the relatively small changes in pore pressure (e.g., Fig. 2) do not appreciably modify this confinement state (for the purposes of Fig. 8). For instance, it was found that use of a G_{max} evaluated at the average confinement over a given stress-strain loop resulted in less than 3% difference for all reported

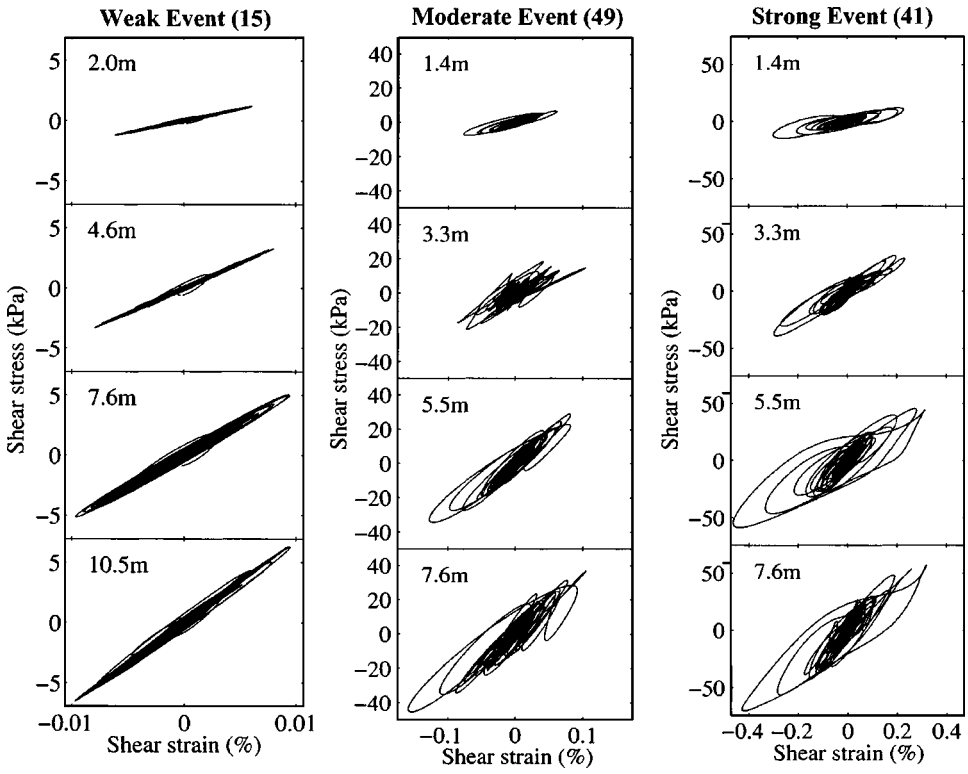

Fig. 3. Shear stress–strain histories identified from recorded accelerations (Events 15, 49, and 41)

G/G_{max} values. Moreover, it is noted that no appreciable change in modulus reduction pattern was observed between the different shaking events investigated.

Fig. 8 also depicts the empirical modulus reduction curves corresponding to the two depths (under drained conditions), as defined by the Hardin–Drnevich equations (1970, 1972). The well known modulus reduction range for sands proposed by Seed–Idriss (1970) is displayed as the shaded region in this figure.

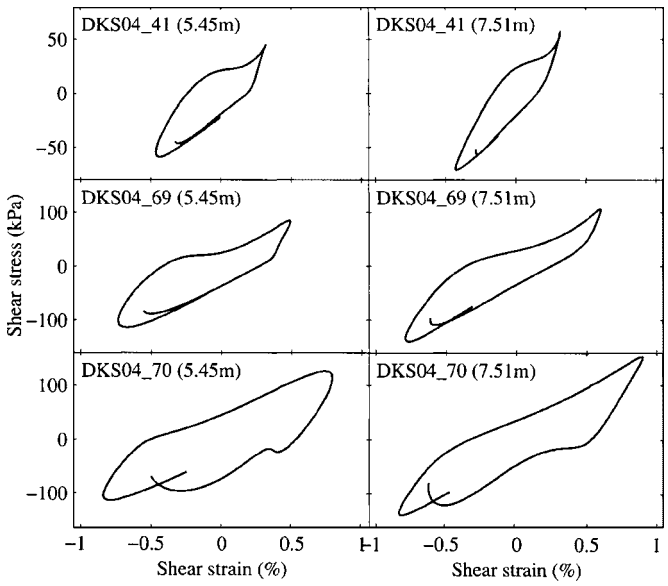

Fig. 4. Shear stress–strain loops showing dilation-induced regain in shear stiffness at large shear strain (events 41, 69, and 70)

As shown in Fig. 8, the experimental data at 7.6 m depth is in good agreement with the corresponding empirical relationships (drained conditions) up to about the 0.1% shear strain level. At 1.4 m depth, the data somewhat lower. More importantly, both the experimental data and the Hardin–Drnevich relations provide a lower band of G/G_{max} variation at the shallower 1.4 m depth (i.e., at the lower confinement). This confinement dependence characteristic was also observed by Stevens (2001) in an analysis of the dense dry sand experiment DKS02, and reported in many earlier studies (e.g., Seed and Idriss 1970, Iwasaki et al. 1978, Kokusho 1980, Ishibashi and Zhang 1993, Silva personal communication 2003).

At shear strain magnitudes higher than about 0.2%, the evaluated modulus reduction is seen to be much less than that dictated by the empirical relations (Fig. 8). This deviation is mainly due to soil dilation effects as discussed above (Figs. 4–6). The dilation of this dense sand under practically undrained conditions kept the shear modulus from further reduction, leveling off at about 20% of its initial value (Fig. 8). It is interesting to note that in 1988, H. B. Seed and J. Sun (Sun personal communications 2004) observed that, even in a dry soil site, a modulus reduction curve with a similar trend (G/G_{max} leveling off at larger shear strains $>1\%$) was needed in order to capture high accleration peaks in the Bonds Corner record (1979 Imperial Valley Earthquake).

Damping Ratio

Fig. 9 shows the damping ratio evaluated from selected stress–strain loops at 1.4 and 7.6 m depths, along with the empirical damping ratio curves of Hardin–Drnevich (1970, 1972), and the sand damping range of Seed–Idriss (shaded area). Considerable scatter exists in the data, but qualitatively the effect of confinement on the damping characteristics is still apparent. In general, damping ratio decreases with the increase in depth (or confine-

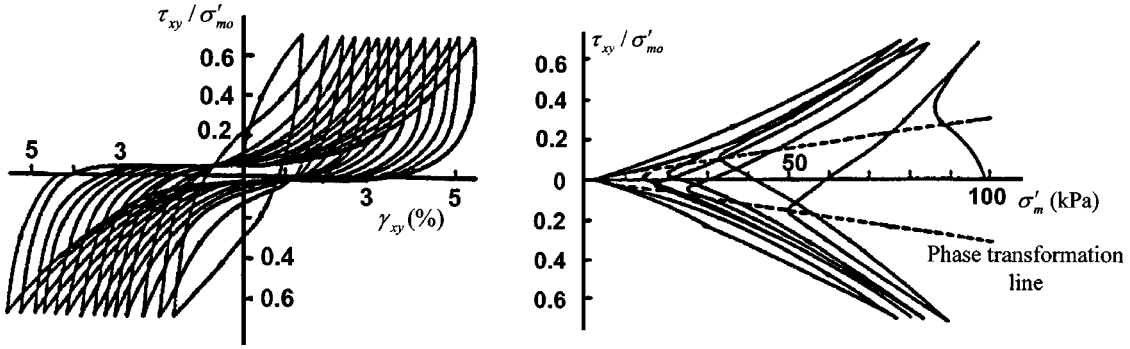

Fig. 5. Undrained torsional shear behavior of Fuji River sand at D_r=75% showing dilation effects (Ishihara 1985) (σ'_m=mean effective confinement; σ'_{m0}=initial mean effective confinement; τ_{xy} and γ_{xy}=in-plane shear stress and strain, respectively)

ment). Such noticeable confinement dependence also appears in the empirical curves of Hardin–Drnevich, with about 5% difference in damping ratio between the two depths (1.4 and 7.6 m), over the strain range of about 0.02–0.2%. This confinement dependence of damping behavior is also in agreement with results reported in earlier studies (e.g., Seed and Idriss 1970, Ishibashi and Zhang 1993, Silva personal communication 2003).

The identified damping ratio data (Fig. 9) is noticeably higher than the corresponding Hardin–Drnevich empirical curves, for shear strains up to about 0.1%. Although the data at 7.6 m depth falls largely inside the range of Seed–Idriss (1970), the data at 1.4 m depth is generally above this range. At this point, no definite reasons for this observed higher damping can be confirmed. Some energy dissipation might be taking place at the container boundaries, but further analysis and investigation is needed to explain and account for this experimental observation.

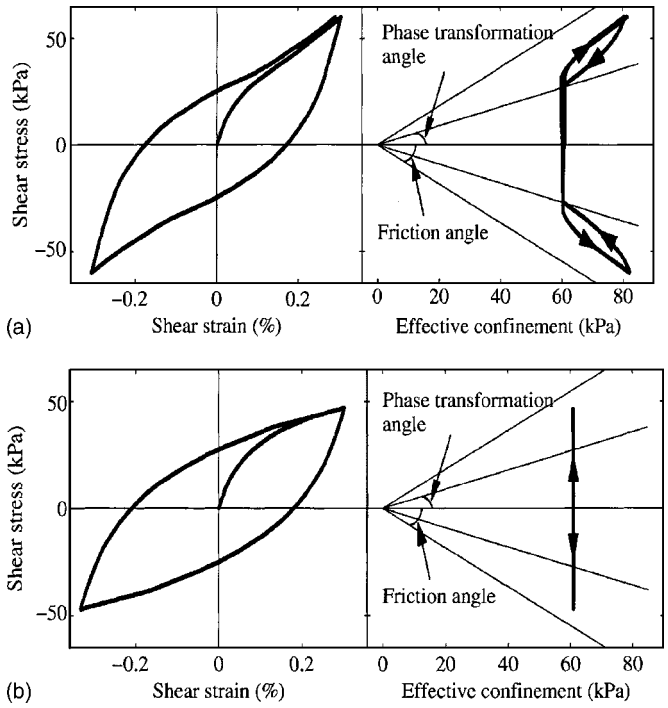

Fig. 6. Schematic of dilatancy effects on shear stress–strain and effective stress path response of dense sands: (a) undrained conditions and (b) drained conditions

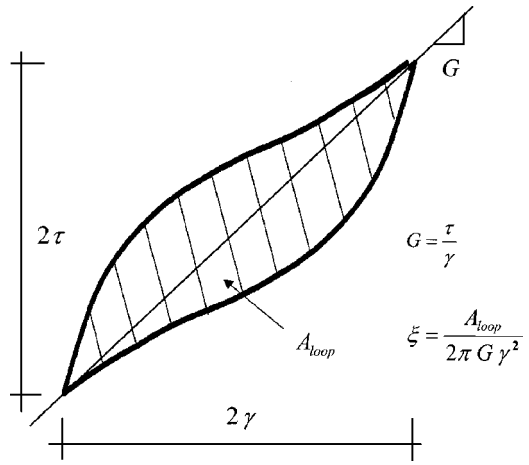

Fig. 7. Schematic for evaluation of shear modulus and damping ratio G and damping ratio ξ from shear stress–strain loop (Kramer 1996)

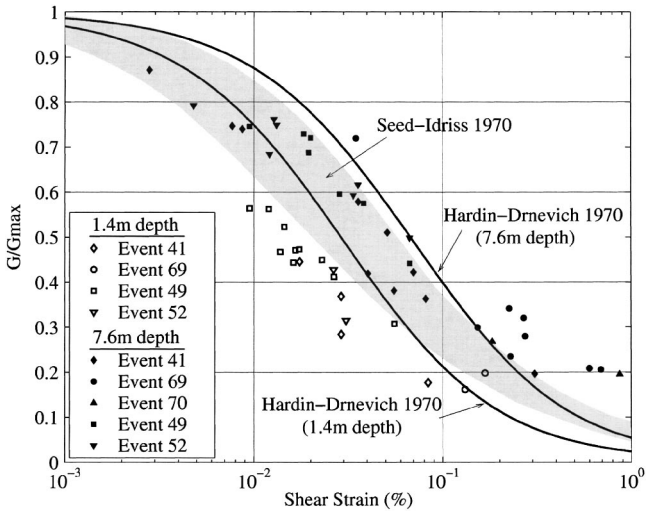

Fig. 8. Identified modulus reduction and empirical relations for saturated dense Nevada sand ($D_r \approx 100\%$)

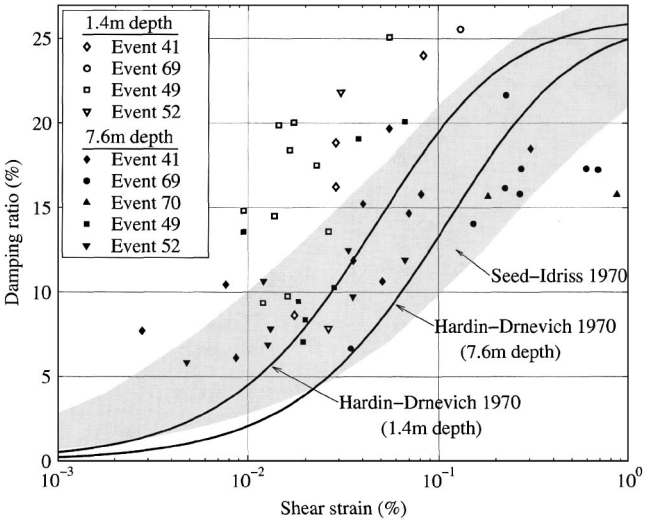

Fig. 9. Identified damping and empirical relations for saturated dense Nevada sand ($D_r \approx 100\%$)

Nevertheless, beyond the 0.2% shear strain, the identified damping levels off, and does not exceed the range of about 20% (or 25% at shallower depth, Fig. 9). This relatively low damping at large strain levels is mainly due to soil dilation as discussed above. In this regard, the stress–strain loops increasingly assume the *S* shape (Figs. 4–6), resulting in lower dissipated energy. Such reduced damping at larger shear strain levels was also observed by Vucetic (1986) and Matasovic and Vucetic (1992, 1993), in undrained direct simple shear testing of five differend sands (at D_r of about 25–75%). In their studies, peak damping ratio (about 20–30%) occurred at a higher shear strain level of about 0.7–1.0%, as those sands were in the looser state. Furthermore, damping ratio of the three denser sands ($D_r \approx 40-75\%$) was observed to actually reduce after reaching the peak value.

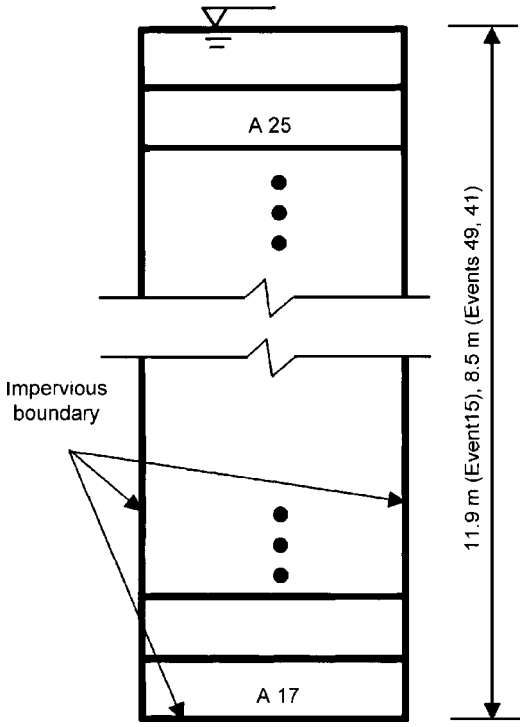

Fig. 10. Finite element model discretization and boundary conditions

Table 3. Main Modeling Parameters for Saturated Dense Nevada Sand ($D_r \approx 100\%$)

Modeling parameter	Parameter value
Low strain shear modulus (kPa)[a]	$G_{max}=30670(z)^{0.5}$
Rayleigh damping coefficients[b]	$a_m=0.0$, $a_k=0.002$ (3.5% average damping ratio over 1–10 Hz range)
Friction angle	42°
Phase transformation angle	22°
Contraction parameter[c]	$c_1=0.007$, $c_2=0.0$
Dilation parameter[d]	$d_1=0.35$, $d_2=10.0$
Permeability (m/s)	$8.25\times10^{-6}\times(g$ level)

[a] z=depth coordinate (m).

[b] a_m and a_k=Rayleigh damping mass and stiffness multipliers, respectively.

[c] c_1 and c_2 values dictate minimal pore-pressure buildup for this very dense sand (see Elgamal et al. 2003).

[d] d_1 and d_2 values control level of soil dilation at large shear strains (see Elgamal et al. 2003).

Summarizing the consistent observations from the available experimental data above (Figs. 2–4, 8, and 9), it may be concluded that dilation prevails in the saturated dense Nevada sand at shear strains higher than 0.2%. This dilation keeps the shear modulus from further reduction below about 20% of its initial value (Fig. 8). The corresponding damping ratio does not exceed about 20–25% (Fig. 9). At low to medium strain levels ($<0.2\%$), the identified modulus reduction patterns are in reasonable agreement with the empirical formulae of Hardin–Drnevich and Seed–Idriss, whereas the estimated damping is higher and requires further investigation. Finally, the identified modulus reduction and damping patterns exhibit noticeable confinement dependence, in agreement with earlier studies.

The experimental data presented above is valuable for calibration and verification of numerical modeling procedures. Particularly, the observed pronounced dilation effects in the strong shak-

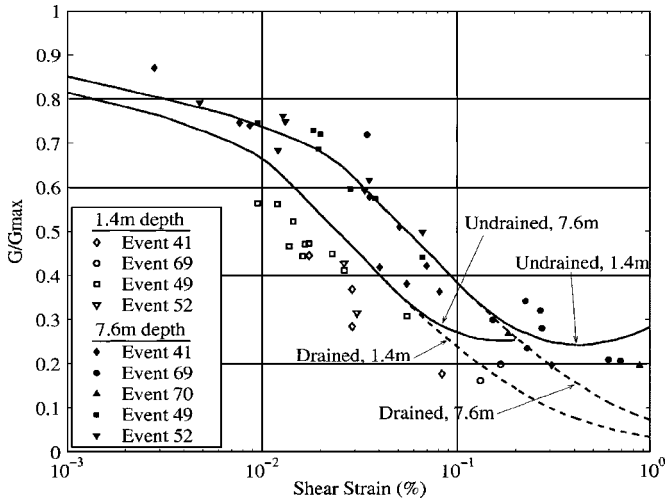

Fig. 11. Model generated modulus reduction curves at different depths for saturated dense Nevada sand ($D_r \approx 100\%$) and data points from centrifuge experiment

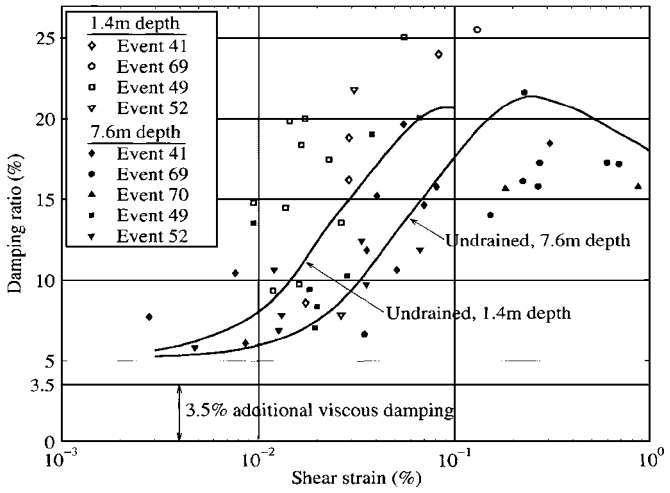

Fig. 12. Overall model damping (including 3.5% viscous damping) at different depths for saturated dense Nevada sand ($D_r \approx 100\%$) and data points from centrifuge experiment

ing events calls for a fully nonlinear site response analysis procedure. In the following, one such numerical approach is calibrated to simulate a representative set of the recorded shaking events.

Numerical Modeling

A 1D effective-stress shear-beam type FE model is employed (Fig. 10). Details of this model and the nonlinear hysteretic stress-strain relationship are described in Appendix I. The modeling effort is focused on matching the observed dense sand response, particularly the highly nonlinear dilative effects. As such, the selected modeling parameters were defined to allow for a numerical response representative of the observed in this experimental program.

Model Calibration

Table 3 lists the main modeling parameters for this saturated dense sand stratum. The initial low-strain shear modulus profile was defined based on the employed shear-wave velocity profile defined earlier. Nonlinearity and dilatancy parameters were selected based on the identified modulus reduction and damping characteristics (Figs. 8 and 9), resulting in a friction angle of 42° and a phase transformation angle of 22°.

The modulus reduction curves generated by the stress-strain model (under undrained conditions) are depicted in Fig. 11, at the initial effective confinements corresponding to 1.4 and 7.6 m depths, respectively. These curves are in reasonable agreement with the experimental data, and show a modulus increase at large shear strain levels. This dilation effect is more pronounced at shallower depths.

As mentioned earlier (Fig. 9), the identified damping was noticeably higher than the range of empirical curves. Consequently, in addition to the hysteretic damping generated by the stress–strain model, viscous (Rayleigh) damping was employed (Fig. 12, Vucetic 1986) with an average of 3.5% over the frequency range of interest (1–10 Hz). Thus, the resulting overall system damping (hysteretic plus viscous) becomes comparable to the experimental

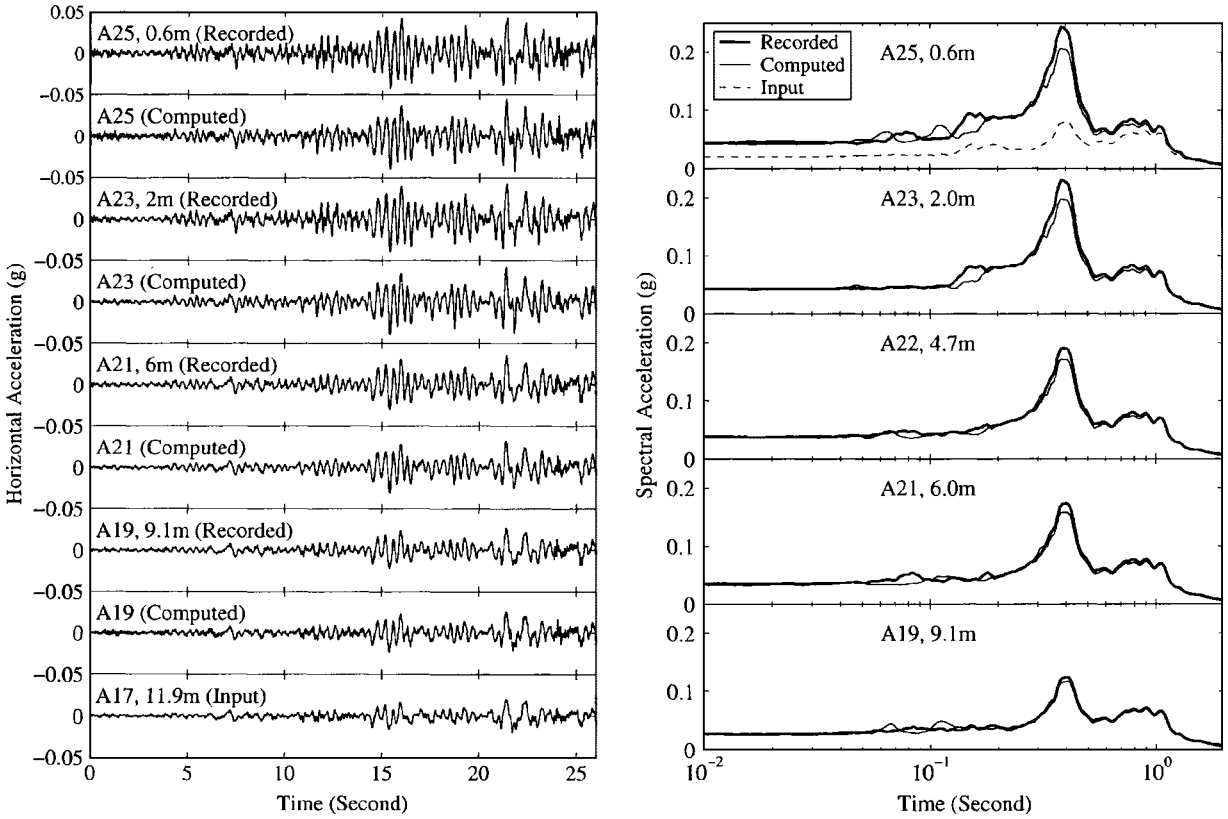

Fig. 13. Event 15 recorded and computed acceleration histories and response spectra (5% damping)

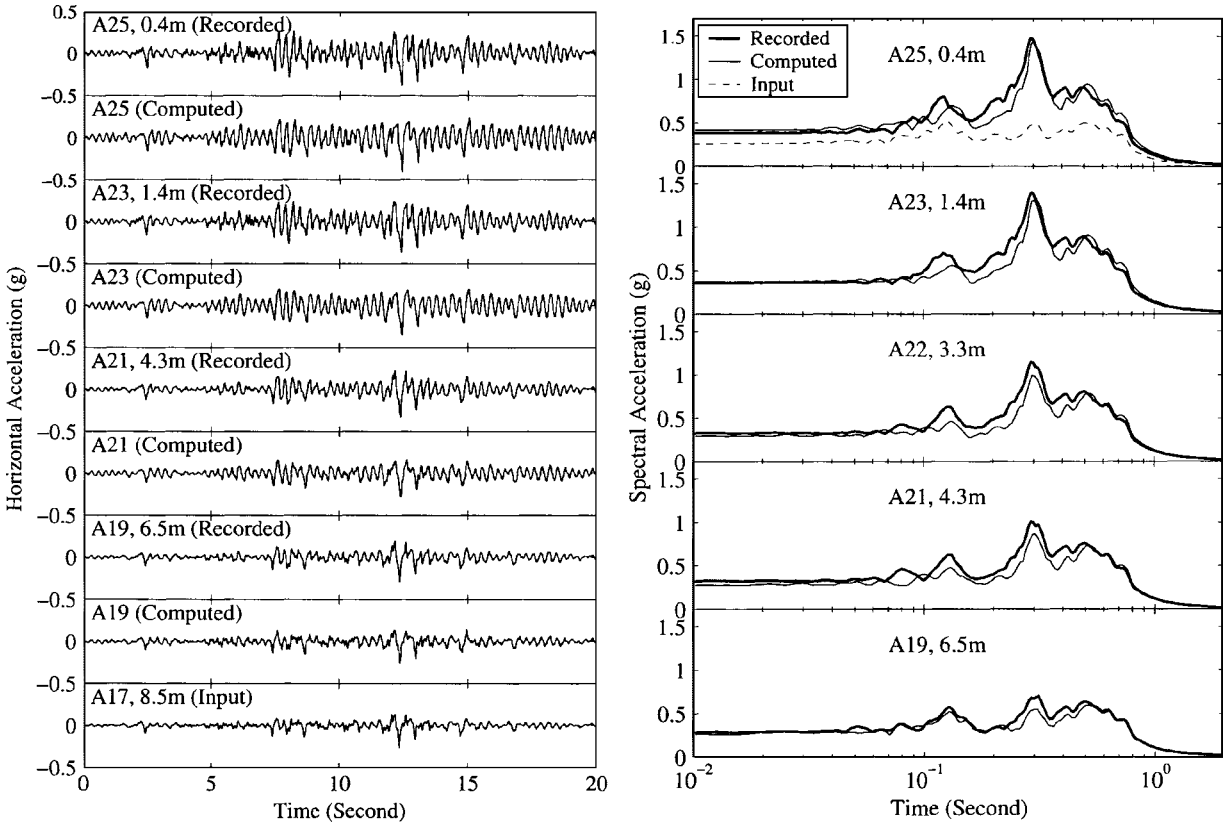

Fig. 14. Event 41 recorded and computed acceleration histories and response spectra (5% damping)

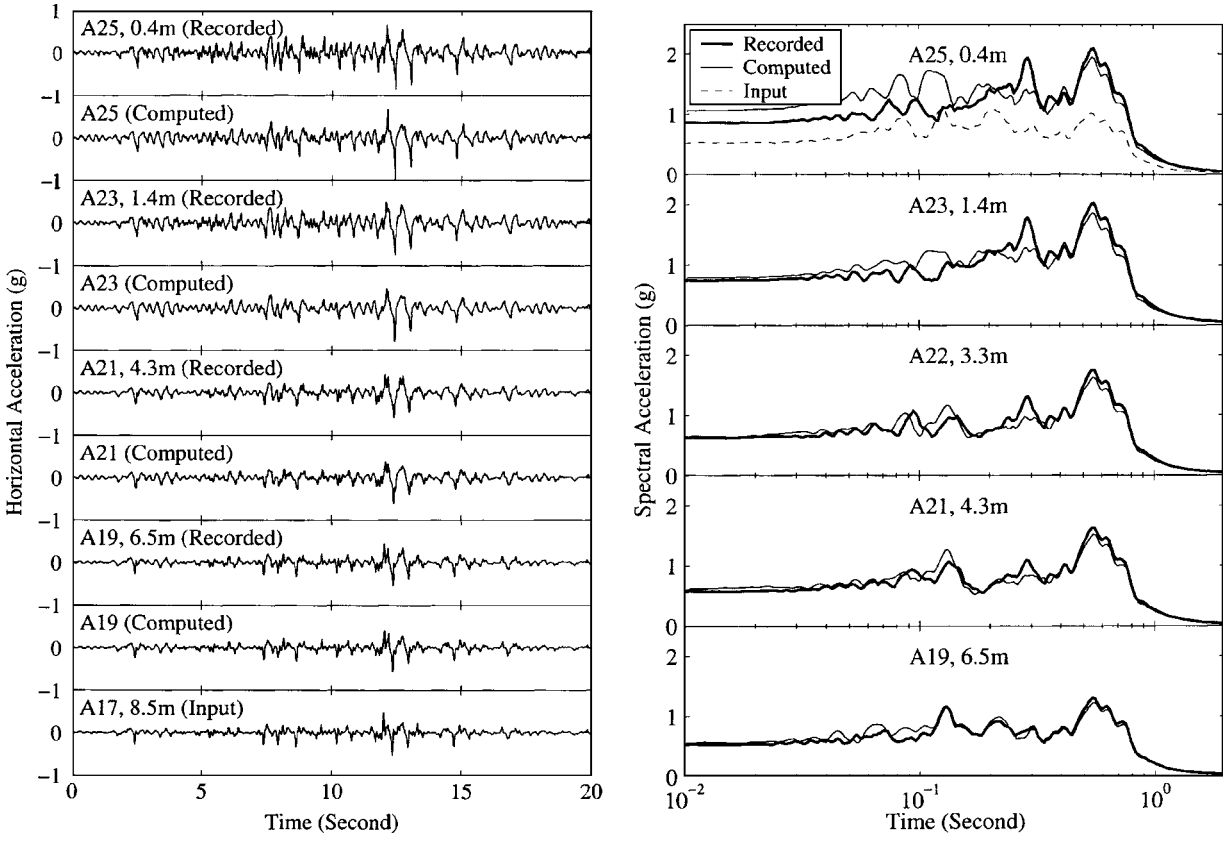

Fig. 15. Event 49 recorded and computed acceleration histories and response spectra (5% damping)

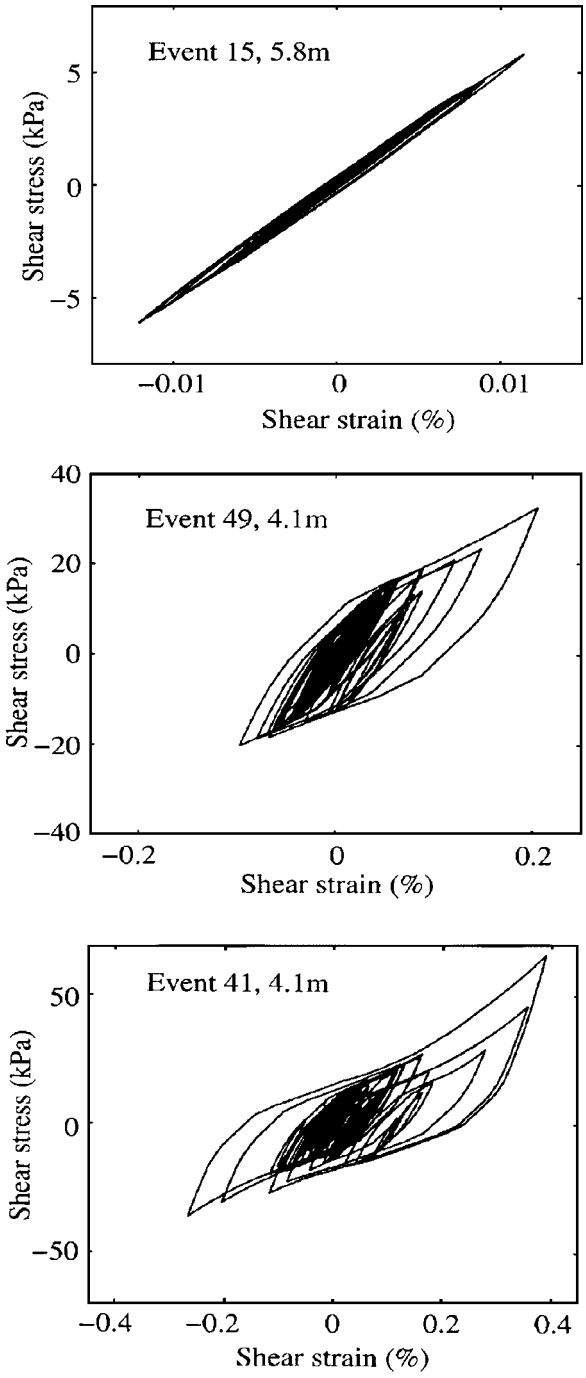

Fig. 16. Computed shear stress–strain response at mid-depth of sand stratum (Events 15, 49, and 41)

data (Fig. 12). As shown in Fig. 12, damping levels off and tends to decrease at large shear strain levels, due to the dilation tendency.

Simulation Results

Representative simulation results of weak, moderate, and strong excitation (Events 15, 49, and 41 respectively) are shown in Figs. 13–15, in terms of acceleration time histories and the corresponding response spectra (5% damping) along the soil profile. In the centrifuge, a prototype stratum of 11.9 m depth was modeled in Event 15 (at 25.3*g*), and 8.5 m depth in Events 49 and 41 (at 18.1*g*). A comparison of the predominant period among these events (from the response spectra) indicates that:

1. The predominant period of the model subjected to Event 15 (about 0.4 s) is longer than that of the model subjected to Event 49 (about 0.3 s). This is attributed mainly to the different prototype stratum depth in these two events (11.9 m in Event 15 and 8.5 m in Event 49).
2. The predominant period in the stronger event (Event 41) is about 0.55 s, longer than that of Event 49 (0.3 s). With the same prototype stratum depth in these two events (8.5 m), the pronounced nonlinear response in Event 41 is seen to have shifted the resonance to a longer period.

In the three cases, the numerical model gives an overall satisfactory match to the experimental counterpart at all accelerometer locations, both in the time and frequency domains. Moreover, the dilation-induced spiky acceleration response observed in Event 41 is reproduced by the numerical model (Fig. 15). In this case, the numerically estimated reduction in mean effective confinement (not shown) ranged from 10% near the model base to about 40% near ground surface, in agreement with the measured pore pressure increase at these locations (Fig. 2).

Fig. 16 shows the computed shear stress–strain histories for all three cases (at mid-depth), with maximum shear strain of about 0.01, 0.1, and 0.4% respectively. Similar to the experimental results (Fig. 3), the computed response indicates: (1) Essentially linear behavior in the low-amplitude event, (2) strong nonlinearity with minor dilatancy effects in the moderate event, and (3) significant presence of strain-stiffening effects due to dilation in the strong event.

Summary and Conclusions

The UCD centrifuge site-response experiment with saturated dense Nevada sand ($D_r \approx 100\%$) produced a comprehensive set of data covering linear to highly nonlinear response scenarios. Assuming a 1D shear beam behavior, shear stress–strain response along the centerline of the sand stratum was calculated from the recorded acceleration time histories. Utilizing this stress–strain data, modulus reduction, damping, and dilatancy characteristics of the soil stratum were identified. Furthermore, numerical simulations were conducted for a representative set of weak to strong shaking events, using a fully coupled nonlinear FE program calibrated by the identification results. The simulation results were in reasonable agreement with the experimental counterparts.

In the small-to-medium strain range ($<0.2\%$), the identified modulus reduction pattern follows approximately the Hardin–Drnevich equations as well as the Seed–Idriss modulus reduction range, while the damping ratio is higher than that predicted by these empirical relationships (further investigation is required). The identified modulus reduction and damping characteristics exhibited a noticeable confinement dependence.

In the large-strain range ($>0.2\%$), the influence of shear-induced dilation was strong (leading to *S*-shaped shear stress–strain loops). As also discussed earlier by Vucetic 1986 and Matasovic and Vucetic 1992, 1993 under the practically undrained loading conditions of this study, the dilation resulted in: (1) instantaneous regain in effective confinement and shear strength, (2) regain in shear stiffness with the increase in shear strain, (3) reduced damping, and (4) pore pressure reduction instants and strong acceleration spikes (approaching about 1.7*g* for some events in this data set). This dilative tendency kept secant shear modulus from reduction below about 20–25% of its initial value, and the corresponding damping ratio from increasing above 20%

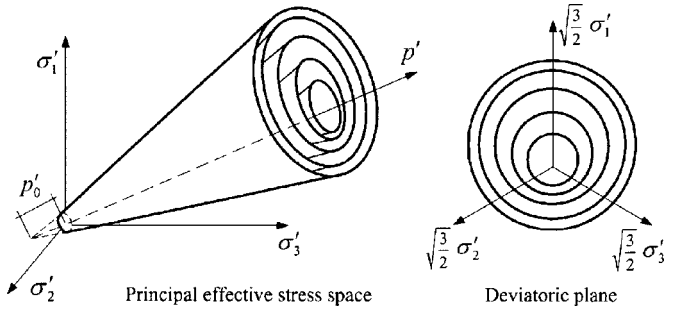

Fig. 17. Conical yield surfaces in principal stress space and deviatoric plane (after Prevost 1985; Elgamal et al. 2003)

approximately. As more data becomes available, these estimates will be further refined.

In this saturated dense sand stratum, the observed response mechanisms may be effectively reproduced by appropriate nonlinear hysteretic models. While the tendency for soil deformation is reduced, an overlying structure might experience instants of very high lateral base acceleration far exceeding 1g. The impact of such input motion on overlying structures should be carefully investigated.

Acknowledgments

The centrifuge model tests were performed at U.C. Davis by Mr. David Stevens (Kleinfelder and Associates) with the assistance of Mr. Byoung-Ill Kim (Myong-Ji University). Mr. James Linjun Yan (U.C. San Diego) and Mr. Garrett Mifsud (California Polytechnic Institute) helped with conducting some of the numerical simulations. Support for this research was provided by the U.S. Geological Survey (USGS) under Award Nos. 99HQGR0019 and 99HQGR0020 (John D. Unger, Manager), and by the Pacific Earthquake Engineering Research Center under Grant No. EEC-9701568 from the National Science Foundation. Partial University of California support (Multi-Campus Research Incentive Fund, MRIF) was provided to initiate this research. This support is gratefully acknowledged.

Appendix I. Numerical Modeling Procedure

Finite Element Formulation

For this study, a plane-strain FE program was employed (Elgamal et al. 2002, Yang and Elgamal 2002), which implements the two-phase (solid and fluid) fully coupled FE formulation of Chan (1988) and Zienkiewicz et al. (1990). The saturated soil is modeled as a two-phase material based on the Biot (1962) theory of porous media. In this FE program, damping is mostly generated from the soil nonlinear hysteretic response. Additional Rayleigh viscous damping may be added if needed.

In this numerical study, a 1D representation of the soil stratum from the surface down to $A17$ (Fig. 1) was defined as a single column of 40 plane-strain elements (Fig. 10). Boundary conditions for all simulations were (Elgamal et al. 2002, Yang and Elgamal 2002):

1. For the solid phase, lateral motion was specified along the base, as the acceleration recorded at $A17$ (Fig. 1). Use of the $A17$ record as input excitation avoids data inconsistency due to potential relative slip between the container base and the soil. To mimic a 1D shear beam effect, displacement degrees of freedom at any given depth were tied together both horizontally and vertically.
2. For the fluid phase, the base and two lateral boundaries were impervious (zero flow rate), with zero pore pressure prescribed at ground surface (i.e., water table at ground surface).
3. Lateral inertia forces were increased by 24% to include the effect of container mass (Stevens et al. 2001 a). The relatively low shear stiffness of the container itself was neglected.

Stress–Strain Model

The FE program incorporates a stress–strain constitutive model developed to reproduce salient soil response characteristics including shear-induced nonlinearity and dilatancy (Figs. 4–6, Parra 1996; Kramer and Elgamal 2001; Elgamal et al. 2003; Yang et al. 2003). This model is based on the framework of multisurface plasticity (Prevost 1985), in which a number of similar conical yield surfaces (36 herein) with different tangent shear moduli were employed to represent shear stress–strain nonlinearity and the confinement dependence of shear stiffness and shear strength (Fig. 17). Shear loading outside the phase transformation surface is accompanied by dilation (Figs. 5 and 6). The outermost surface is the envelope of peak shear strength (failure envelope).

Model calibration is typically based on matching a given backbone shear stress–strain curve at a particular level of confinement. Once calibrated, the conical yield surface configuration restrictively defines stress–strain response at all other confinement levels (i.e., within the current model, shear stress–strain relationship cannot be independently defined for depths of 1.4 and 7.6 m for instance, Figs. 8 and 9). Therefore, an effort must be made to maintain reasonable accuracy within the overall confinement level of interest.

References

Arulmoli, K., Muraleetharan, K. K., Hossain, M. M., and Fruth, L. S. (1992). "VELACS: Verification of liquefaction analyses by centrifuge studies, laboratory testing program, soil data report." Rep. Prepared for The Earth Technology Corporation, *Project No. 90-0562*, Irvine, Calif.

Biot, M. A. (1962). "The mechanics of deformation and acoustic propagation in porous media." *J. Appl. Phys.*, 33(4), 1482–1498.

Chan, A. H. C. (1988). "A unified finite element solution to static and dynamic problems in geomehanics." P.D dissertation, Univ. College of Swansea, Swansea, U.K.

Elgamal, A., and Lai, T. (2001). "Comprehensive investigation of nonlinear site response—collaborative research with UC san diego, and UC Davis." *Final Technical Rep. to USGS*, Dept. of Structural Engineering, Univ. of California at San Diego, San Diego.

Elgamal, A., Lai, T., Yang, Z., and He, L. (2001). "Dynamic soil properties, seismic downhole arrays and applications in practice." *State-of-the-Art Paper, Proc., 4th Int. Conf. on Recent Advances in Geotechnical Earthquake Engineering and Soil Dynamics*, S. Prakash, ed., San Diego.

Elgamal, A., Yang, Z., and Parra, E. (2002). "Computational modeling of cyclic mobility and post-liquefaction site response." *Soil Dyn. Earthquake Eng.*, 22(4), 259–271.

Elgamal, A., Yang, Z., Parra, E., and Ragheb, A. (2003). "Modeling of cyclic mobility in saturated cohesionless soils." *Int. J. Plast.*, 19(6), 883–905.

Elgamal, A.-W.. Zeghal, M., and Parra, E. (1996). "Liquefaction of reclaimed island in Kobe, Japan." *J. Geotech. Eng.,* 122(1), 39–49.

Field, E. H., et al. (1998). "Nonlinear site response: Where we're at, a report from a SCEC/PEER seminar and workshop." *Seismol. Res. Lett.,* 69(3), 230–234.

Hardin, B. O., and Drnevich, V. P. (1970). "Shear modulus and damping in soils-II: Design equations and curves." *Univ. of Kentucky Technical Rep. No. UKY 27-70-CE3, Soil Mechanics Series No. 2*, 49. Univ. of Kentucky, Lexington, Ky.

Hardin, B. O., and Drnevich, V. P. (1972). "Shear modulus and damping in soils." *J. Soil Mech. Found. Div.,* 98(7), 667–692.

Ishihara, K. (1985). "Stability of natural deposits during earthquakes." *Proc., 11th Int. Conf. on Soil Mechanics and Foundation Engineering*, Vol. 2, San Francisco, 321–376.

Ishihara, K., Tatsuoka, F., and Yasuda, S. (1975). "Undrained deformation and liquefaction of sand under cyclic stresses." *Soils Found.,* 15(1), 29–44.

Ishibashi, I., and Zhang, X. (1993). "Unified dynamic shear moduli and damping ratios of sand and clay." *Soils Found.,* 33(1), 182–191.

Iwasaki, T., Tatsuoka, F., and Takagi, Y. (1978). "Shear modulus of sands under torsional shear loading." *Soils Found.,* 18(1), 39–56.

Koga, Y., and Matsuo, O. (1990). "Shaking table tests of embankments resting on liquefiable sandy ground." *Soils Found.,* 30(4), 162–174.

Kokusho, T. (1980). "Cyclic triaxial test of dynamic soil properties for wide strain range." *Soils Found.,* 20(2), 45–60.

Kramer, S. L. (1996). *Geotechnical earthquake engineering*, Prentice Hall, Upper Saddle River, N.J.

Kramer, S. L., and Elgamal, A.-W. (2001). "Modeling soil liquefaction hazards for performance-based earthquake engineering." *Rep. No. 2001/13*, Pacific Earthquake Engineering Research Center, Univ. of California, Berkeley, Calif.

Kutter, B. L. (1992). "Dynamic centrifuge modeling of geotechnical structures." *Transp. Res. Rec. 1336*, National Research Council, Transportaion Research Board, Washington, D.C., 24–30.

Kutter, B. L., Li, X. S., Sluis, W., and Cheney, J. A. (1991). "Performance and instrumentation of the large centrifuge at UC Davis." *Centrifuge 91*, Ko and McLean, eds., Balkema, Rotterdam, The Netherlands, 19–26.

Kutter, B. L., and Wilson, D. W. (1999). "De-liquefaction shock waves." *Proc., 7th U.S.–Japan Workshop on Earthquake Resistant Design of Lifeline Facilities and Countermeasures Against Soil Liquefaction, Rep. MCEER-99-0019*, Seattle, T. O'Rourke, J. P. Bardet, and M. Hamada. eds., 295–310.

Lai, T., Elgamal, A., Wilson, D. W., and Kutter B. L.. (2001). "Numerical modeling for site seismic response in laminated centrifuge container." *Proc., 1st Albert CAQUOT Int. Conf.*, Paris.

Lai, T., Elgamal, A., Wilson, D. W., and Kutter, B. L. (2002). "Three-dimensional modeling for site seismic response in laminated and rigid centrifuge containers." *Proc., Int. Conf. on Physical Modeling in Geotechnics*, St. John's, NF, Canada.

Lambe, T. W., and Whitman, R. V. (1969). *Soil mechanics*, Wiley, New York

Matasovic, N. and Vucetic, M. (1992). "Modeling of the cycle stress-strain behavior of liquefiable sands." *Research Report* , Dept. of Civil Engineering, Univ. of California at Los Angeles, Los Angeles, Calif.

Matasovic, N. and Vucetic, M. (1993). "Cyclic characterization of liquefiable sands."*J. Geotech. Eng.,* 119(11), 1805–1822

Parra, E. (1996). "Numerical modeling of liquefaction and lateral ground deformation including cyclic mobility and dilation response in soil system." PhD thesis, Rensselaer Polytechnic Institute, Troy, N.Y.

Prevost, J. H. (1985). "A simple plasticity theory for frictional cohesionless soils." *Soil Dyn. Earthquake Eng.,* 4(1), 9–17.

Seed, H. B., and Idriss, I. M. (1970). "Soil moduli and damping factors for dynamic response analyses." *Rep. No. EERC-70/10*, Earthquake Engineering Research Center, Univ. of California at Berkeley, Berkeley, Calif.

Stevens, D. K. (2001). "Dynamic site response of dense sand centrifuge models." Master thesis, Univ. of California at Davis, Davis, Calif.

Stevens, D. K., Wilson, D. W., and Kutter, B. L. (2001a). "Comprehensive investigation of nonlinear site response—Centrifuge data report for the DKS04 model test." *Rep. No. UCD/CGMDR-01/03*, Dept. of Civil and Environmental Engineering, Univ. of California at Davis, Davis, Calif.

Stevens, D. K., Wilson, D. W., Kutter, B. L., Kim, B. I., and Elgamal, A. (2001b). "Centrifuge model tests to identify dynamic properties of dense sand for site response calculations." *Proc., 4th Int. Conf. on Recent Advances in Geotechnical Earthquake Engineering and Soil Dynamics*, S. Prakash, ed., San Diego.

Vucetic, M. (1986). "Pore pressure buildup and liquefaction of level sandy sites during earthquakes." PhD thesis, Rensselaer Polytechnic Institute, Troy, N.Y.

Yang, Z., and Elgamal, A. (2002). "Influence of permeability on liquefaction-induced shear deformation." *J. Eng. Mech.,* 128(7), 720–729.

Yang, Z., Elgamal, A., and Parra, E. (2003). "Computational model for cyclic mobility and associated shear deformation." *J. Geotech. Geoenviron. Eng.,* 129(12), 1119–1127.

Zeghal, M., Elgamal, A.-W., Tang, H. T., and Stepp, J. C. (1995). "Lotung downhole array. II: Evaluation of Soil Nonlinear properties." *J. Geotech. Eng.,* 121(4), 363–378.

Zienkiewicz, O. C., Chan, A. H. C., Pastor, M., Paul, D. K., and Shiomi, T. (1990). "Static and dynamic behavior of soils: A rational approach to quantitative solutions: I. Fully saturated problems." *Proc. R. Soc. London, Ser. A* 429, 285–309.